Chinese Journal of Aeronautics, (2013),26(6): 1430–1438

Chinese Society of Aeronautics and Astronautics
& Beihang University

Chinese Journal of Aeronautics

cja@buaa.edu.cn
www.sciencedirect.com

Transient aeroelastic responses and flutter analysis of a variable-span wing during the morphing process

Huang Ren, Qiu Zhiping *

Institute of Solid Mechanics, Beihang University, Beijing 100191, China

Received 26 September 2012; revised 6 December 2012; accepted 14 January 2013
Available online 1 August 2013

KEYWORDS

Galerkin methods;
Morphing aircraft;
Time-varying systems;
Transient aeroelastic;
Unsteady vortex lattice method;
Variable-span wing

Abstract To investigate the transient aeroelastic responses and flutter characteristics of a variable-span wing during the morphing process, a novel first-order state-space aeroelastic model is proposed. The time-varying structural model of the morphing wing is established based on the Euler–Bernoulli beam theory with time-dependent boundary conditions. A nondimensionalization method is used to translate the time-dependent boundary conditions to be time-independent. The time-domain aerodynamic forces are calculated by the reduced-order unsteady vortex lattice method. The morphing parameters, i.e., wing span length and morphing speed, are of particular interest for understanding the fundamental aeroelastic behavior of variable-span wings. A test case is proposed and numerical results indicate that the flutter characteristics are sensitive to both of the two morphing parameters. It could be noticed that the aeroelastic characteristics during the wing extracting process are more serious than those during the extending process at the same morphing speed by transient aeroelastic response analysis. In addition, a faster morphing process can get better aeroelastic performance while the mechanism comlexity will arise.

1. Introduction

Morphing aircrafts, which will lead to the next generation of multi-mission aircrafts, have been a significant topic in aerospace research recently.[1–5] The variable-span wing morphing concept is to change an aircraft's wing span during flight. As a result, the wing area and aspect ratio are changeable for different flight conditions to obtain the optimal lift-to-drag ratio. Aeroelastic problems with morphing can be described as the interaction between the time-dependent/configuration-varying aerodynamics and the structure. Time-varying or transient aeroelastic responses and flutter analysis during the morphing process become very important due to the rapid and large-scale morphing motion. To meet the tremendous challenges, effective theoretical models and computational methodologies should be developed.

In previous work, several researchers focused on the morphing aeroelastic problems, especially on the folding-wing (Z-wing) concept.[6–11] The continuous morphing process was divided into several steady steps in most of the previous studies, and the morphing velocity was not taken into account. The complex task conditions require the morphing process to be as efficient as possible. Hence, the steady-state analysis methods are no longer applicable for the rapid morphing process

* Corresponding author. Tel.: +86 10 82339638.
E-mail addresses: huangren@buaa.edu.cn (R. Huang), zpqiu@buaa.edu.cn (Z. Qiu).

Peer review under responsibility of Editorial Committee of CJA.

ELSEVIER Production and hosting by Elsevier

http://dx.doi.org/10.1016/j.cja.2013.07.047

due to the time-varying characteristics of the aeroelastic system.[12]

The multi-body dynamics approach was usually undertaken to obtain the equations of motion of the morphing wing.[13,14] However, for the variable-span wing concept, the multi-body simulation fails because the wing configuration is continuous and not easily decomposed into components.

Bae et al.[15] conducted the aerodynamic and static aeroelastic characteristics analysis of a variable-span missile wing. The finite element method and the panel method were used to obtain the structural model and the aerodynamic model, respectively. Only the impact of span length is investigated. Wang HB and Wang HP[16] established an aeroelastic model based on the Timoshenko beam theory and the supersonic piston aerodynamic theory. The effect trend of the axis morphing speed on the flutter speed was discussed.

In the present study, a variable-length, Euler–Bernoulli beam model is combined with the reduced-order unsteady vortex lattice aerodynamic model to develop a first-order, state-space model for transient aeroelastic analysis of the variable-span wing during the morphing process. Effects of the changing wing span and various morphing velocities on the flutter speed and frequency are investigated. Furthermore, transient aeroelastic responses are also studied.

2. Structural model

A morphing unmanned aerial vehicle with different configurations is shown in Fig. 1. In this study, half of the variable-span wing is described as a cantilever Euler–Bernoulli beam, whose length $l(t)$ is time-dependent. The chord length is assumed to be constant along the span-wise and expressed as $2b$. The half span length of the original wing is l_0. The morphing process can be simplified as an extending or contracting process of the beam at velocity $\dot{l}(t)$.

The bending displacement in the z direction and torsion rotation about the y-axis of the wing are denote by w and θ. The external loads acting on the wing are represented by a force L per unit length and applied to the symmetrical points of cross-section together with a torque M_{ea} per unit length respectively. With the uniformity assumption, one can express the governing equations of vertical deflection and pitching motion by using the Hamilton principle, as follows:

$$\begin{cases} m\dfrac{\partial^2 w}{\partial t^2} - mx_\alpha\dfrac{\partial^2\theta}{\partial t^2} + \mathrm{EI}\dfrac{\partial^4 w}{\partial y^4} = L \\ -mx_\alpha\dfrac{\partial^2 w}{\partial t^2} + mr_\alpha^2\dfrac{\partial^2\theta}{\partial t^2} - \mathrm{GJ}\dfrac{\partial^2\theta}{\partial y^2} = M_{ea}. \end{cases} \tag{1}$$

where EI and GJ are the bending and torsional rigidity of the wing, respectively, m is the mass per unit length, x_α is the distance coefficient of the gravity center to the elastic axis, and r_α is the radius of gyration about the elastic axis.

The boundary conditions are split into two groups: three boundary conditions come from the clamped end and the other three from the free end. The latter are time-dependent:

$$\frac{\partial^2 w(l(t),t)}{\partial y^2} = \frac{\partial^3 w(l(t),t)}{\partial y^3} = \frac{\partial\theta(l(t),t)}{\partial y} = 0 \tag{2}$$

To deal with the above time-varying boundary condition problem, a nondimensionalization method is proposed to translate a time-dependent item into a time-independent one.

Introduce the following basic non-dimensional parameters:

$$\tilde{y} = y(t)/l(t), \quad \tilde{x} = x/b, \quad \tilde{w}(\tilde{y},t) = w(y,t)/b, \quad \tilde{\theta}(\tilde{y},t) = \theta(y,t), \quad \tilde{x}_\alpha = x_\alpha/b, \quad \tilde{r}_\alpha = r_\alpha/b, \quad l(t) = l_0\alpha(t),$$

and Eq. (1) can be cast in the following dimensionless form

$$\begin{cases} [\alpha^4\ddot{\tilde{w}} + 2\dot{\alpha}\alpha^3(1-\tilde{y})\dot{\tilde{w}}' + \alpha^2(\ddot{\alpha}\alpha - \dot{\alpha}^2) \\ \cdot(1-\tilde{y})\tilde{w}' + \alpha^2\dot{\alpha}^2(1-\tilde{y})^2\tilde{w}''] - \tilde{x}_\alpha[\alpha^4\ddot{\tilde{\theta}} \\ +2\dot{\alpha}\alpha^3(1-\tilde{y})\dot{\tilde{\theta}}' + \alpha^2(\ddot{\alpha}\alpha - \dot{\alpha}^2)(1-\tilde{y})\tilde{\theta}' \\ +\alpha^2\dot{\alpha}^2(1-\tilde{y})^2\tilde{\theta}''] + k_w^2\tilde{w}'''' = \alpha^4 L/mb \\ -\tilde{x}_\alpha[\alpha^4\ddot{\tilde{w}} + 2\dot{\alpha}\alpha^3(1-\tilde{y})\dot{\tilde{w}}' + \alpha^2(\ddot{\alpha}\alpha - \dot{\alpha}^2) \\ \cdot(1-\tilde{y})\tilde{w}' + \alpha^2\dot{\alpha}^2(1-\tilde{y})^2\tilde{w}''] + \tilde{r}_\alpha^2[\alpha^4\ddot{\tilde{\theta}} \\ +2\dot{\alpha}\alpha^3(1-\tilde{y})\dot{\tilde{\theta}}' + \alpha^2(\ddot{\alpha}\alpha - \dot{\alpha}^2)(1-\tilde{y})\tilde{\theta}' \\ +\alpha^2\dot{\alpha}^2(1-\tilde{y})^2\tilde{\theta}''] - k_\theta^2\tilde{\theta}'' = \alpha^4 M_{ea}/mb^2, \end{cases} \tag{3}$$

where primes and dots denote differentiation with respect to dimensionless position $\tilde{y}$ and time t, respectively; α is the dimensionless half span length; $\dot{\alpha}$ are the dimensionless morphing speed. $k_w = \sqrt{\mathrm{EI}/(ml_0^4)}$ and $k_\theta = \sqrt{\mathrm{GJ}/(ml_0^2b^2)}$ are, respectively, the dimensionless bending rigidity coefficient and torsional rigidity coefficient.

The dimensionless boundary condition at the free end becomes time-independent

$$\tilde{w}''(1,t) = \tilde{w}'''(1,t) = \tilde{\theta}'(1,t) = 0 \tag{4}$$

The time-dependent governing differential equations of the beam are fourth-order nonlinear hyperbolic partial differential equations, whose exact solution cannot be easily obtained. A Galerkin method would be introduced to get an approximate solution with the aerodynamic loads in Section 4.

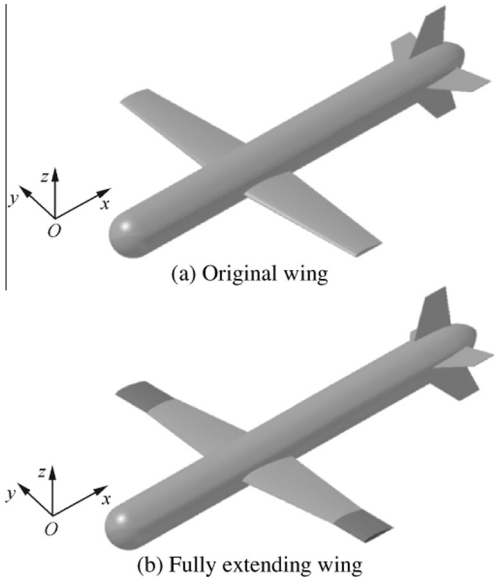

Fig. 1 An unmanned aerial vehicle with variable-span wings.

3. Reduced-order aerodynamic model

Fig. 2 shows the aerodynamic loads acting on the airfoil with a flight speed V. The unsteady aerodynamic forces per unit length can be obtained using a two-dimensional reduced-order unsteady

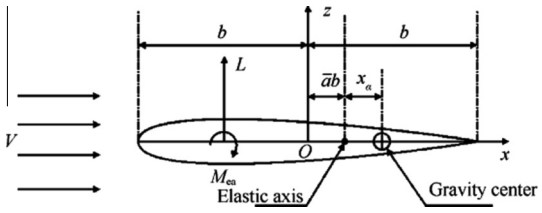

Fig. 2 Aerodynamic loads acting on the airfoil.

vortex lattice method.[17] The model of unsteady vortex lattice describes the unsteady aerodynamic forces in time domain, which is not limited to the assumption of harmonic motion.[18]

In the unsteady vortex lattice model, the airfoil is divided into M elements representing the bound vortices, and the wake is divided into $N-M$ elements as the free vortices. The total number of vortices on both the airfoil and the wake is N. The element are all of equal size Δx in the streamwise direction. The most important boundary condition requiring zero normal velocity across the solid boundaries can be expressed as a dimensionless form

$$\tilde{\boldsymbol{W}}_{3/4} = \begin{bmatrix} \tilde{\boldsymbol{K}}_{\mathrm{b}} & \tilde{\boldsymbol{K}}_{\mathrm{w}} \end{bmatrix} \begin{bmatrix} \tilde{\boldsymbol{\Gamma}}_{\mathrm{b}} \\ \tilde{\boldsymbol{\Gamma}}_{\mathrm{w}} \end{bmatrix} \tag{5}$$

where the vector $\tilde{\boldsymbol{W}}_{3/4}$ represents the dimensionless downwash at the collocation points of the vortex elements on the airfoil section. $\tilde{\boldsymbol{\Gamma}}_{\mathrm{b}}$ and $\tilde{\boldsymbol{\Gamma}}_{\mathrm{w}}$ are the dimensionless strength vectors of the bound vortices and the free vortices, respectively. The kernel functions $\tilde{\boldsymbol{K}}_{\mathrm{b}}$ and $\tilde{\boldsymbol{K}}_{\mathrm{w}}$ can be defined by using Biot-Savart's law.

The aerodynamic governing equations in continuous time domain can be written as

$$\boldsymbol{A}_{\mathrm{c}}\dot{\tilde{\boldsymbol{\Gamma}}}_{\mathrm{w}} = \frac{V_0}{\Delta\tilde{x}}\boldsymbol{B}_{\mathrm{c}}\tilde{\boldsymbol{\Gamma}}_{\mathrm{w}} + \boldsymbol{D}_{\mathrm{c}}\dot{\tilde{\boldsymbol{W}}}_{3/4} \tag{6}$$

where $V_0 = V/b$ is the dimensionless flight speed, $\Delta\tilde{x} = \Delta x/b$ is the dimensionless element size, and

$$\boldsymbol{A}_{\mathrm{c}} = \begin{bmatrix} \boldsymbol{S} \\ \boldsymbol{0} \end{bmatrix} \tilde{\boldsymbol{K}}_{\mathrm{b}}^{-1}\tilde{\boldsymbol{K}}_{\mathrm{w}} + \begin{bmatrix} 0 & \boldsymbol{0} \\ \boldsymbol{0} & \boldsymbol{I}_{N-M-1} \end{bmatrix},$$

$$\boldsymbol{D}_{\mathrm{c}} = \begin{bmatrix} \boldsymbol{S} \\ \boldsymbol{0} \end{bmatrix} \tilde{\boldsymbol{K}}_{\mathrm{b}}^{-1}, \boldsymbol{B}_{\mathrm{c}} = \boldsymbol{A}_{\mathrm{c}}\ln(\boldsymbol{A}_{\mathrm{d}}^{-1}\boldsymbol{B}_{\mathrm{d}}), \quad \boldsymbol{A}_{\mathrm{d}} = \boldsymbol{I} - \begin{bmatrix} \boldsymbol{S} \\ \boldsymbol{0} \end{bmatrix} \tilde{\boldsymbol{K}}_{\mathrm{b}}^{-1}\tilde{\boldsymbol{K}}_{\mathrm{w}},$$

$$\boldsymbol{B}_{\mathrm{d}} = \begin{bmatrix} \boldsymbol{0}_{1\times(N-M)} \\ \boldsymbol{C} \end{bmatrix} - \begin{bmatrix} \boldsymbol{S} \\ \boldsymbol{0} \end{bmatrix} \tilde{\boldsymbol{K}}_{\mathrm{b}}^{-1}\tilde{\boldsymbol{K}}_{\mathrm{w}}, \quad \boldsymbol{S} = [\,1 \quad 1\cdots 1 \quad 1\,]_{1\times M},$$

$$\boldsymbol{C} = \begin{bmatrix} 1 & & & \\ & 1 & & \\ & & \ddots & \\ & & & 1 \quad \sigma \end{bmatrix}, \quad \sigma = 0.996,$$

$\boldsymbol{I}$ is a unity matrix.

A lot of attentions are paid to reduced-order models for applications in aeroelastic systems.[19] A modal reduction method for extracting the most important aerodynamic modes is used in this study.

The unsteady solution can be decomposed into two parts. One takes the static effect of the neglected eigenmodes, and the other determines the dynamic part, i.e.,

$$\tilde{\boldsymbol{\Gamma}}_{\mathrm{w}} = \boldsymbol{\Psi}_R\boldsymbol{q} + \tilde{\boldsymbol{\Gamma}}_{\mathrm{s}} \tag{7}$$

where $\boldsymbol{\Psi}_R$ is a $(N-M)\times R$ matrix whose columns are the R columns of the eigenvectors of the matrix $\boldsymbol{A}_{\mathrm{c}}^{-1}\boldsymbol{B}_{\mathrm{c}}$ corresponding to the first R eigenvalues most close to the origin. q is the new generalized coordinate vector. The static correction item $\tilde{\boldsymbol{\Gamma}}_{\mathrm{s}}$ can be expressed in the following form

$$\tilde{\boldsymbol{\Gamma}}_{\mathrm{s}} = \frac{\Delta\tilde{x}}{V_0}(-\boldsymbol{B}_{\mathrm{c}}^{-1} + \boldsymbol{\Psi}_R\boldsymbol{\Lambda}_R\boldsymbol{\Phi}_R^{\mathrm{T}}\boldsymbol{A}_{\mathrm{c}}^{-1})\boldsymbol{D}_{\mathrm{c}}\dot{\tilde{\boldsymbol{W}}}_{3/4} = \frac{\Delta\tilde{x}}{V_0}\boldsymbol{K}_{\mathrm{c}}\boldsymbol{D}_{\mathrm{c}}\dot{\tilde{\boldsymbol{W}}}_{3/4} \tag{8}$$

where $\boldsymbol{K}_{\mathrm{c}} = -\boldsymbol{B}_{\mathrm{c}}^{-1} + \boldsymbol{\Psi}_R\boldsymbol{\Lambda}_R\boldsymbol{\Phi}_R^{\mathrm{T}}\boldsymbol{A}_{\mathrm{c}}^{-1}$, $\boldsymbol{\Lambda}_R$ is an $R\times R$ sub-matrix whose non-zero entries are those of the eigenvalue matrix of $\boldsymbol{A}_{\mathrm{c}}^{-1}\boldsymbol{B}_{\mathrm{c}}$ corresponding to the R retained eigenvalues, and $\boldsymbol{\Phi}_R$ is a matrix whose column of the left eigenvectors of $\boldsymbol{A}_{\mathrm{c}}^{-1}\boldsymbol{B}_{\mathrm{c}}$ corresponding to the first R eigenvalues most close to the origin.

By using the unsteady Bernoulli equation, the unsteady lift L and the moment M_{ea} can be written as

$$\begin{cases} L = \rho_{\mathrm{a}}b^3\left(V_0\sum\limits_{i=1}^{M}\tilde{\Gamma}_{\mathrm{b},i} + \sum\limits_{i=1}^{M}\sum\limits_{j=1}^{i}\dot{\tilde{\Gamma}}_{\mathrm{b},j}\Delta\tilde{x}\right) \\ M_{\mathrm{ea}} = -\rho_{\mathrm{a}}b^4\left[V_0\sum\limits_{i=1}^{M}(\tilde{x}_{\mathrm{vb},i} - \bar{a})\tilde{\Gamma}_{\mathrm{b},i}\right. \\ \qquad \left. + \sum\limits_{i=1}^{M}(\tilde{x}_{\mathrm{vb},i} - \bar{a})\sum\limits_{j=1}^{i}\dot{\tilde{\Gamma}}_{\mathrm{b},j}\Delta\tilde{x}\right] \end{cases} \tag{9}$$

where $\tilde{x}_{\mathrm{vb},i}$ is the dimensionless location of the ith bound vortex, $\tilde{\Gamma}_{\mathrm{b},i}$ is the dimensionless strength of the ith bound vortex. $\bar{a}$ is the distance coefficient of the mid chord to the elastic axis, and ρ_{a} is the air density.

On the basis of Eq. (9), the right-hand side terms in Eq. (3) can be rewritten as

$$\begin{cases} L_1 = \dfrac{\alpha^4 L}{mb} = \dfrac{\alpha^4}{\pi\mu}(V_0\boldsymbol{F}_1\tilde{\boldsymbol{\Gamma}}_{\mathrm{b}} + \boldsymbol{F}_2\dot{\tilde{\boldsymbol{\Gamma}}}_{\mathrm{b}}) \\ M_1 = \dfrac{\alpha^4 M_{\mathrm{ea}}}{mb^2} = \dfrac{\alpha^4}{\pi\mu}(V_0\boldsymbol{G}_1\tilde{\boldsymbol{\Gamma}}_{\mathrm{b}} + \boldsymbol{G}_2\dot{\tilde{\boldsymbol{\Gamma}}}_{\mathrm{b}}) \end{cases} \tag{10}$$

where

$$\boldsymbol{F}_1 = [\,11 \quad \cdots 1 \quad 1\,]_{1\times M}, \quad \boldsymbol{F}_2 = \Delta\tilde{x}\cdot\boldsymbol{F}_1\cdot\mathrm{tril}(1)_{M\times M},$$

$$\boldsymbol{G}_1 = -[\,(\tilde{x}_{\mathrm{vb},1} - \bar{a}) \quad (\tilde{x}_{\mathrm{vb},2} - \bar{a})\cdots \quad (\tilde{x}_{\mathrm{vb},M} - \bar{a})\,]_{1\times M},$$

$$\boldsymbol{G}_2 = \Delta\tilde{x}\cdot\boldsymbol{G}_1\cdot\mathrm{tril}(1)_{M\times M}, \quad \mu = m/\pi\rho_{\mathrm{a}}b^2$$

is the mass ratio, and $\mathrm{tril}(1)_{M\times M}$ is a lower triangular matrix whose nonzero elements are all equal to 1.

At the collocation points of the vortex elements, the downwash velocity arising from the unsteady motion of the airfoil can be written as

$$\boldsymbol{W}_{3/4} = -\boldsymbol{S}^{\mathrm{T}}\dot{w} + \boldsymbol{D}_{\mathrm{a}}\dot{\tilde{\theta}} + V_0\boldsymbol{S}^{\mathrm{T}}\tilde{\theta}. \tag{11}$$

where $\boldsymbol{D}_{\mathrm{a}} = [\,(\tilde{x}_{\mathrm{c},1} - \bar{a}) \quad (\tilde{x}_{\mathrm{c},2} - \bar{a})\cdots \quad (\tilde{x}_{\mathrm{c},M} - \bar{a})\,]^{\mathrm{T}}$, and $\tilde{x}_{\mathrm{c},i}$ is the dimensionless location of the ith collocation point.

Combining Eqs. (5), (7), (8) with Eq. (10), the aerodynamic loads can be expressed as the following forms

$$\begin{cases} L_1 = \dfrac{\alpha^4}{\pi\mu}\left(H_1\ddot{\tilde{w}} + H_2\ddot{\tilde{\theta}} + V_0H_3\dot{\tilde{w}} + V_0H_4\dot{\tilde{\theta}}\right. \\ \qquad \left. + V_0^2H_5\tilde{\theta} + \boldsymbol{H}_6\dot{\boldsymbol{q}} + V_0\boldsymbol{H}_7\boldsymbol{q}\right) \\ M_1 = \dfrac{\alpha^4}{\pi\mu}\left(J_1\ddot{\tilde{w}} + J_2\ddot{\tilde{\theta}} + V_0J_3\dot{\tilde{w}} + V_0J_4\dot{\tilde{\theta}}\right. \\ \qquad \left. + V_0^2J_5\tilde{\theta} + \boldsymbol{J}_6\dot{\boldsymbol{q}} + V_0\boldsymbol{J}_7\boldsymbol{q}\right), \end{cases} \tag{12}$$

where the coefficients $H_1\sim H_5$, $J_1\sim J_5$, and the matrices $\boldsymbol{H}_6$, $\boldsymbol{H}_7$, $\boldsymbol{J}_6$, and $\boldsymbol{J}_7$ are listed in Appendix.

4. State-space aeroelastic model

The dimensionless aeroelastic equations can be obtained by combining the aerodynamic loads and the structural model. By introducing the modal analytic techniques, the bending and torsion deformations can be represented in the terms of truncated series,[20] as follows:

$$\begin{cases} \tilde{w}(\tilde{y},t)=\sum_{i=1}^{N_w} v_i(\tilde{y})\eta_i(t)=\boldsymbol{v\eta} \\ \tilde{\theta}(\tilde{y},t)=\sum_{i=1}^{N_\theta} \Theta_i(\tilde{y})\beta_i(t)=\boldsymbol{\Theta\beta} \end{cases} \tag{13}$$

The governing equations may be rewritten in terms of the mode shapes as the following

$$\begin{cases} \alpha^4\boldsymbol{v}\ddot{\boldsymbol{\eta}}+2\dot{\alpha}\alpha^3(1-\tilde{y})\boldsymbol{v}'\dot{\boldsymbol{\eta}}+\alpha^2(\ddot{\alpha}\alpha-\dot{\alpha}^2) \\ \cdot(1-\tilde{y})\boldsymbol{v}'\boldsymbol{\eta}+\alpha^2\dot{\alpha}^2(1-\tilde{y})^2\boldsymbol{v}''\boldsymbol{\eta}-\tilde{x}_\alpha\big[\alpha^4\boldsymbol{\Theta}\ddot{\boldsymbol{\beta}} \\ +2\dot{\alpha}\alpha^3(1-\tilde{y})\boldsymbol{\Theta}'\dot{\boldsymbol{\beta}}+\alpha^2(\ddot{\alpha}\alpha-\dot{\alpha}^2)(1-\tilde{y})\boldsymbol{\Theta}'\boldsymbol{\beta} \\ +\alpha^2\dot{\alpha}^2(1-\tilde{y})^2\boldsymbol{\Theta}''\boldsymbol{\beta}\big]+k_w^2\boldsymbol{v}''''\boldsymbol{\eta}=L_1 \\ -\tilde{x}_\alpha[\alpha^4\boldsymbol{v}\ddot{\boldsymbol{\eta}}+2\dot{\alpha}\alpha^3(1-\tilde{y})\boldsymbol{v}'\dot{\boldsymbol{\eta}}+\alpha^2(\ddot{\alpha}\alpha-\dot{\alpha}^2) \\ \cdot(1-\tilde{y})\boldsymbol{v}'\boldsymbol{\eta}+\alpha^2\dot{\alpha}^2(1-\tilde{y})^2\boldsymbol{v}''\boldsymbol{\eta}+\tilde{r}_\alpha^2\big[\alpha^4\boldsymbol{\Theta}\ddot{\boldsymbol{\beta}} \\ +2\dot{\alpha}\alpha^3(1-\tilde{y})\boldsymbol{\Theta}'\dot{\boldsymbol{\beta}}+\alpha^2(\ddot{\alpha}\alpha-\dot{\alpha}^2)(1-\tilde{y})\boldsymbol{\Theta}'\boldsymbol{\beta} \\ +\alpha^2\dot{\alpha}^2(1-\tilde{y})^2\boldsymbol{\Theta}''\boldsymbol{\beta}\big]-k_\theta^2\boldsymbol{\Theta}''\boldsymbol{\beta}=M_1. \end{cases} \tag{14}$$

Using Eqs. (12) and (13), the right-hand side terms of the above equations are expressed as follows

$$\begin{cases} L_1=\dfrac{\alpha^4}{\pi\mu}\big(H_1\boldsymbol{v}\ddot{\boldsymbol{\eta}}+H_2\boldsymbol{\Theta}\ddot{\boldsymbol{\beta}}+V_0H_3\boldsymbol{v}\dot{\boldsymbol{\eta}}+V_0H_4\boldsymbol{\Theta}\dot{\boldsymbol{\beta}} \\ \qquad +V_0^2H_5\boldsymbol{\Theta}\boldsymbol{\beta}+\boldsymbol{H}_6\dot{\boldsymbol{q}}+V_0\boldsymbol{H}_7\boldsymbol{q}\big) \\ M_1=\dfrac{\alpha^4}{\pi\mu}\big(J_1\boldsymbol{v}\ddot{\boldsymbol{\eta}}+J_2\boldsymbol{\Theta}\ddot{\boldsymbol{\beta}}+V_0J_3\boldsymbol{v}\dot{\boldsymbol{\eta}}+V_0J_4\boldsymbol{\Theta}\dot{\boldsymbol{\beta}} \\ \qquad +V_0^2J_5\boldsymbol{\Theta}\boldsymbol{\beta}+\boldsymbol{J}_6\dot{\boldsymbol{q}}+V_0\boldsymbol{J}_7\boldsymbol{q}\big). \end{cases} \tag{15}$$

Using the Galerkin method, multiplying the first equations of Eqs. (14) and (15) by $\boldsymbol{v}^{\mathrm{T}}$ and the second equations of Eqs. (14) and (15) by $\boldsymbol{\Theta}^{\mathrm{T}}$, integrating over the dimensionless span, while taking into account the initial conditions, the governing equations can be written in a matrix form as

$$\begin{aligned}&(\boldsymbol{M}_{\mathrm{s}}+\boldsymbol{M}_{\mathrm{a}})\ddot{\boldsymbol{\xi}}+(\boldsymbol{C}_{\mathrm{s}}+V_0\boldsymbol{C}_{\mathrm{a}})\dot{\boldsymbol{\xi}}+(\boldsymbol{K}_{\mathrm{s}}+V_0^2\boldsymbol{K}_{\mathrm{a}})\boldsymbol{\xi} \\ &\quad+\boldsymbol{D}\dot{\boldsymbol{q}}+V_0\boldsymbol{E}\boldsymbol{q}=\boldsymbol{0}\end{aligned} \tag{16}$$

where $\boldsymbol{\xi}=[\,\boldsymbol{\eta}^{\mathrm{T}}\quad\boldsymbol{\beta}^{\mathrm{T}}\,]^{\mathrm{T}}$ is the vector of the generalized structural coordinates, and the terms of the above matrices and vectors are defined in Appendix.

Especially, for Eq. (6), combined with Eqs. (7) and (8), the aerodynamic governing equations are recast into the following forms

$$\begin{aligned}\boldsymbol{I}_R\dot{\boldsymbol{q}}+\frac{\Delta\tilde{x}}{V_0}\boldsymbol{\Phi}_R^{\mathrm{T}}\boldsymbol{K}_{\mathrm{c}}\boldsymbol{D}_{\mathrm{c}}\ddot{\boldsymbol{W}}_{3/4}&=\frac{V_0}{\Delta\tilde{x}}\boldsymbol{\Lambda}_R\boldsymbol{q}+\boldsymbol{\Phi}_R^{\mathrm{T}}\boldsymbol{A}_{\mathrm{c}}^{-1}\boldsymbol{B}_{\mathrm{c}}\boldsymbol{K}_{\mathrm{c}}\boldsymbol{D}_{\mathrm{c}}\dot{\boldsymbol{W}}_{3/4} \\ &\quad+\boldsymbol{\Phi}_R^{\mathrm{T}}\boldsymbol{A}_{\mathrm{c}}^{-1}\boldsymbol{D}_{\mathrm{c}}\dot{\tilde{\boldsymbol{W}}}_{3/4}.\end{aligned} \tag{17}$$

where $\boldsymbol{I}_R$ is a $R\times R$ identity matrix.

Substituting Eq. (13) into Eq. (11), neglecting the higher-order derivative terms, multiplying both sides by $\boldsymbol{\Theta}^{\mathrm{T}}$, and integrating over the dimensionless span, the downwash velocity can be rewritten as

$$\tilde{\boldsymbol{W}}_{3/4}=\boldsymbol{A}_{14}\dot{\boldsymbol{\xi}}+V_0\boldsymbol{A}_{15}\boldsymbol{\xi}. \tag{18}$$

where

$$\boldsymbol{A}_{14}=\frac{1}{\boldsymbol{S}\boldsymbol{A}_{13}}[[-\boldsymbol{S}^{\mathrm{T}},\quad\cdots,\quad-\boldsymbol{S}^{\mathrm{T}}]\boldsymbol{A}_1^{\mathrm{T}},[\boldsymbol{D}_a,\quad\cdots,\quad\boldsymbol{D}_a]\boldsymbol{I}_{N_\theta}],$$

$$\boldsymbol{A}_{15}=\frac{1}{\boldsymbol{S}\boldsymbol{A}_{13}}[[\boldsymbol{0},\quad\cdots,\quad\boldsymbol{0}],[\boldsymbol{S}^{\mathrm{T}},\quad\cdots,\quad\boldsymbol{S}^{\mathrm{T}}]\boldsymbol{I}_{N_\theta}],$$

and the matrix $\boldsymbol{A}_{13}$ is list in Appendix.

Substituting Eq. (18) into Eq. (17), one can obtain the aerodynamic governing equations as

$$\boldsymbol{I}_R\dot{\boldsymbol{q}}+\boldsymbol{A}_{\boldsymbol{q}}\ddot{\boldsymbol{\xi}}=\frac{V_0}{\Delta\tilde{x}}\boldsymbol{\Lambda}_R\boldsymbol{q}+V_0\boldsymbol{B}_{\boldsymbol{q}}\dot{\boldsymbol{\xi}}. \tag{19}$$

where

$$\begin{aligned}&\boldsymbol{A}_{\boldsymbol{q}}=\Delta\tilde{x}\boldsymbol{\Phi}_R^{\mathrm{T}}\boldsymbol{K}_{\mathrm{c}}\boldsymbol{D}_{\mathrm{c}}\boldsymbol{A}_{15}-\boldsymbol{\Phi}_R^{\mathrm{T}}\boldsymbol{A}_{\mathrm{c}}^{-1}\boldsymbol{B}_{\mathrm{c}}\boldsymbol{K}_{\mathrm{c}}\boldsymbol{D}_{\mathrm{c}}\boldsymbol{A}_{14}-\boldsymbol{\Phi}_R^{\mathrm{T}}\boldsymbol{A}_{\mathrm{c}}^{-1}\boldsymbol{D}\boldsymbol{A}_{14}, \\ &\boldsymbol{B}_{\boldsymbol{q}}=\boldsymbol{\Phi}_R^{\mathrm{T}}\boldsymbol{A}_{\mathrm{c}}^{-1}\boldsymbol{B}_{\mathrm{c}}\boldsymbol{K}_{\mathrm{c}}\boldsymbol{D}_{\mathrm{c}}\boldsymbol{A}_{15}+\boldsymbol{\Phi}_R^{\mathrm{T}}\boldsymbol{A}_{\mathrm{c}}^{-1}\boldsymbol{D}_{\mathrm{c}}\boldsymbol{A}_{15}.\end{aligned}$$

Based on Eqs. (16) and (19), a first-order aeroelastic state-space model is developed and can be expressed as

$$\begin{cases} \boldsymbol{A}\dot{\boldsymbol{X}}=\boldsymbol{B}\boldsymbol{X}+\boldsymbol{C}\boldsymbol{U} \\ \boldsymbol{Y}=\boldsymbol{D}\boldsymbol{X} \end{cases} \tag{20}$$

where the state variable vector and system matrices are

$$\mathbf{X}=\begin{bmatrix}\alpha\\ \boldsymbol{q}\\ \boldsymbol{\xi}\\ \dot{\boldsymbol{\xi}}\end{bmatrix},\quad \boldsymbol{A}=\begin{bmatrix}\boldsymbol{0}&\boldsymbol{0}&\boldsymbol{0}&\boldsymbol{0}\\ \boldsymbol{0}&\boldsymbol{I}_R&\boldsymbol{0}&\boldsymbol{A}_{\boldsymbol{q}}\\ \boldsymbol{0}&\boldsymbol{0}&\boldsymbol{I}_{N_w+N_\theta}&\boldsymbol{0}\\ \boldsymbol{0}&\boldsymbol{D}&\boldsymbol{0}&\boldsymbol{M}_s+\boldsymbol{M}_a\end{bmatrix},$$

$$\boldsymbol{B}=\begin{bmatrix}\boldsymbol{0}&\boldsymbol{0}&\boldsymbol{0}&\boldsymbol{0}\\ \boldsymbol{0}&\frac{V_0}{\Delta\tilde{x}}\boldsymbol{\Lambda}_R&\boldsymbol{0}&V_0\boldsymbol{B}_{\boldsymbol{q}}\\ \boldsymbol{0}&\boldsymbol{0}&\boldsymbol{0}&\boldsymbol{I}_{N_w+N_\theta}\\ \boldsymbol{0}&-V_0\boldsymbol{E}&-(\boldsymbol{K}_{\mathrm{s}}+V_0^2\boldsymbol{K}_{\mathrm{a}})&-(\boldsymbol{C}_s+V_0\boldsymbol{C}_{\mathrm{a}})\end{bmatrix},$$

$$\boldsymbol{C}=[1\quad\boldsymbol{0}\quad\boldsymbol{0}\quad\boldsymbol{0}]^{\mathrm{T}},\quad\boldsymbol{U}=\{\dot{\alpha}\},\boldsymbol{Y}=\{\boldsymbol{\xi}\},\boldsymbol{D}=[\boldsymbol{0}\quad\boldsymbol{0}\quad\boldsymbol{I}_{N_w+N_\theta}\quad\boldsymbol{0}].$$

In the present study, the flutter analysis of the variable-span wing with different configurations $\alpha(t)$ and different morphing velocities $\dot{\alpha}(t)$ will adopt the generalized aeroelastic analysis method,[21] and the governing equations can be written as

$$[s\boldsymbol{I}-\overline{\boldsymbol{A}}^{-1}(s)\overline{\boldsymbol{B}}(s)]\boldsymbol{X}(s)=\boldsymbol{0}. \tag{21}$$

where

$$\overline{\boldsymbol{A}}=\begin{bmatrix}\boldsymbol{I}_R&\boldsymbol{0}&\boldsymbol{A}_{\boldsymbol{q}}\\ \boldsymbol{0}&\boldsymbol{I}_{N_w+N_\theta}&\boldsymbol{0}\\ \boldsymbol{D}&\boldsymbol{0}&\boldsymbol{M}_{\mathrm{s}}+\boldsymbol{M}_{\mathrm{a}}\end{bmatrix},$$

$$\overline{\boldsymbol{B}}=\begin{bmatrix}\frac{V_0}{\Delta\tilde{x}}\boldsymbol{\Lambda}_R&\boldsymbol{0}&V_0\boldsymbol{B}_{\boldsymbol{q}}\\ \boldsymbol{0}&\boldsymbol{0}&\boldsymbol{I}_{N_w+N_\theta}\\ -V_0\boldsymbol{E}&-(\boldsymbol{K}_{\mathrm{s}}+V_0^2\boldsymbol{K}_{\mathrm{a}})&-(\boldsymbol{C}_{\mathrm{s}}+V_0\boldsymbol{C}_{\mathrm{a}})\end{bmatrix}.$$

The eigenvalue solving method in MATLAB is used to determine the system stability of the morphing wing. The aeroelastic formulations have the state-space form which is suitable for the use of the MATLAB ordinary differential equation solver.[22]

5. Numerical results

5.1. Solution verification

Given that the current aeroelastic model for a variable-span wing configuration is relatively complicated, various special cases in which the system reduces to something more familiar have been compared with known literature solutions. In the present study, the special case of $\alpha(t) = 1$ and $\dot{\alpha}(t) = 0$ is computed according to the parameters used for the Goland wing.[23] The bending and pitching mode shapes of the wing are introduced by Hodeges and Pierce,[24] and the first fourth-order modes are used for aeroelastic analysis. The reduced-order model of aerodynamics is constructed by using a total of 20 eigen modes. The flutter speed and frequency of the current model are 133 m/s and 72.7 rad/s, respectively, which are compared with 137 m/s and 70.7 rad/s of the original Goland wing. The error relative to that given by Goland is less than 3%.

5.2. Flutter analysis of a non-morphing wing

A test case is considered to demonstrate the results of the model and analysis. The parameters listed in Table 1 are representatives of a physical model when the wing span is non-morphing. The full extension reaches up to 50% increase in wing span relative to the original configuration, i.e., $\alpha(t) \in [1.0, 1.5]$. The absolute value of the dimensionless morphing velocity $\dot{\alpha}(t)$ can vary between 0.1 and 0.5, i.e., the morphing process can proceed from 10 s to 2 s. Furthermore, the morphing process is assumed as a uniform motion.

The flutter speed of the non-morphing wing is 77 m/s and the flutter frequency is about 149.6 rad/s. Fig. 3 shows the root loci as a function of airspeed between 1 m/s and 100 m/s. For clarity, only the region near the origin is presented. The influence of velocity on the aerodynamic eigenvalues is regular. Meanwhile, the tendency of structural eigenvalues with airspeed increasing is evident. The flutter mode is the second mode.

5.3. Flutter analysis for different wing span lengths

Figs. 4 and 5 show the flutter speed and frequency varying with the length of the wing span, and the transient morphing speed is assumed as zero. From the original configuration to the fully extending wing, both the critical flutter speed and frequency decrease significantly, the flutter speed drops from 77 m/s to 34.2 m/s, and the flutter frequency from 149.6 rad/s to 66.5 rad/s. Meanwhile, the descending speed becomes slow when the wing span increases. The flexibility of the wing is arising when the aspect ratio increases during the morphing process, which is the most important influencing factor on the aeroelastic characteristics of a variable-span wing. The flutter mode does not change because the cross-sectional variations are ignored in this study.

Table 1 Basic data of the variable-span wing.

Parameters	Value
Basic half span (m)	3
Chord (m)	1
Mass per unit length (kg/m)	6
Spanwise elastic axis (m)	35% of chord
Gravity center (m)	45% of chord
Mass moment of inertia (kg·m)	0.75
Torsional rigidity (N·m^2)	6×10^4
Bending rigidity (N·m^2)	6×10^5

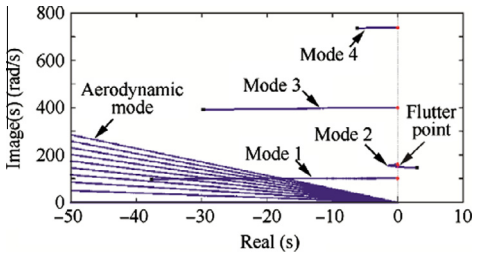

Fig. 3 Root loci of non-morphing wing flutter analysis.

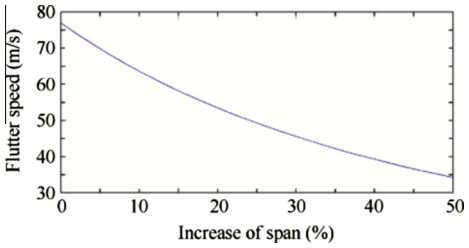

Fig. 4 Flutter speed vs. wing span length.

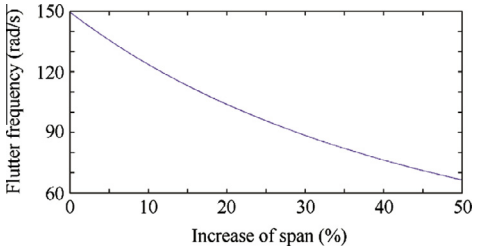

Fig. 5 Flutter frequency vs. wing span length.

5.4. Flutter analysis for different morphing speeds

In this case, the impacts of the morphing speed to the flutter characteristics are considered as the configuration is fixed. Two configurations with a wing span of 1.1 times and 1.4 times of the original span length are studied, respectively. The dimensionless morphing speed $\dot{\alpha}(t)$ varies between -0.5 and 0.5, and the wing is at a contracting process when $\dot{\alpha}(t)$ is minus. Figs. 6 and 7 show the flutter speeds for different morphing speeds in the two configurations. As a result, the flutter speeds

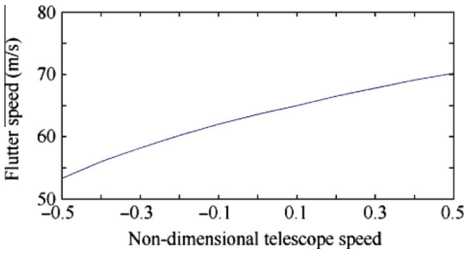

Fig. 6 Flutter speed vs. morphing speed ($\alpha = 1.1$).

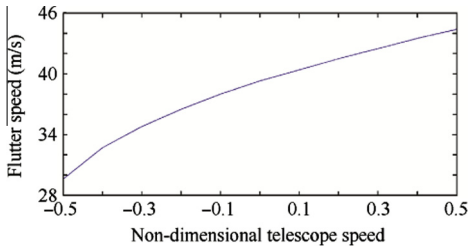

Fig. 7 Flutter speed vs. morphing speed ($\alpha = 1.4$).

increase in both configurations with the increasing of the morphing speed. Taking into account the ascent speed of the flutter speed, one can find that the impact of the morphing speed on the aeroelastic characteristics is more serious in the shorter wing length configurations than in the longer ones.

Figs. 8 and 9 indicate the root loci as a function of airspeed at the highest morphing speed in both configurations, and one can find that the starting points of the root loci move away from the image axis farther, which indicates that the structural properties change with the morphing speed. Let us recall the aeroelastic governing equations, i.e., Eq. (16) and Eqs. (A15–A22). In mathematical terms, the impacts of the morphing speed $\dot{\alpha}$ on the aeroelastic system are reflected in the structural damping matrix $\boldsymbol{C}_s$ and the structural rigidity matrix $\boldsymbol{K}_s$. The influences on the structural stiffness would be neglected as the terms $k_w^2\boldsymbol{A}_7$ and $k_\theta^2\boldsymbol{A}_{11}$, which are the structural rigidity matrix terms of a non-morphing wing, are three orders of magnitude larger than other terms due to $\dot{\alpha}$. However, in the matrix $\boldsymbol{C}_s$, the terms are proportional to the morphing speed $\dot{\alpha}$ if the wing length α is fixed. A faster morphing speed would lead to an increase of structural damping during the wing extending process, which would delay the flutter phenomenon occurring and lead to an increase of the transient flutter speed. This tendency would reverse during the contracting process as the morphing speed $\dot{\alpha}(t)$ is minus.

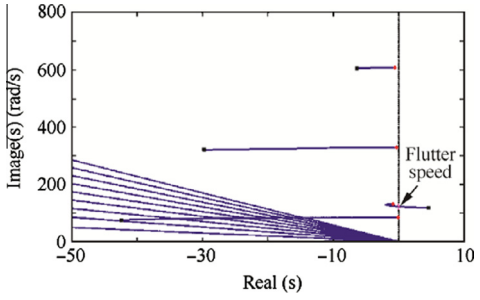

Fig. 8 Root loci of the morphing wing ($\alpha = 1.1, \dot{\alpha} = 0.5$).

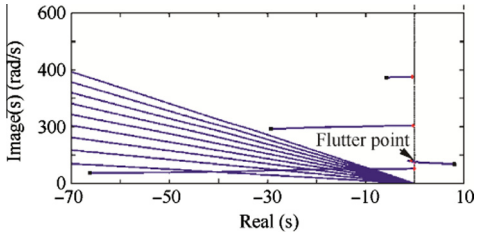

Fig. 9 Root loci of the morphing wing ($\alpha = 1.4, \dot{\alpha} = 0.5$).

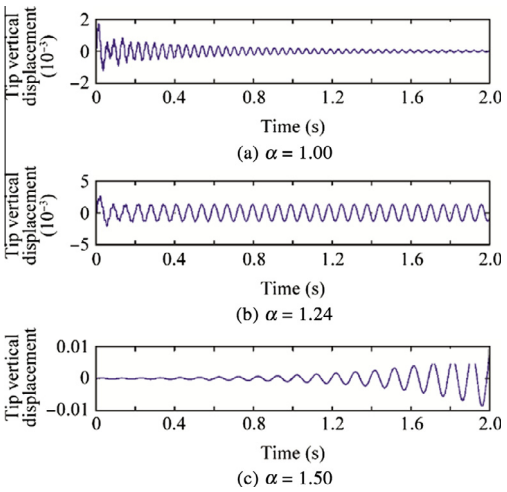

Fig. 10 Tip vertical displacement responses with different configurations ($V = 50$ m/s).

5.5. Transient aeroelastic responses

The time histories of oscillations with span lengths of l_0 and $1.5l_0$ at a flight speed of 50 m/s are obtained. The configurations are both fixed. The dimensionless tip vertical displacements and tip twist are plotted against time in Figs. 10 and 11. The amplitudes of oscillation decay with a span length of l_0 while grow with the $1.5l_0$ configuration. A critical state, i.e., a periodic oscillation, is observed with a span length of $1.24l_0$ so that the flight speed of 50 m/s should be the flutter speed predicted by the present model. The responses with the span length of $1.5l_0$ indicated in Figs. 10 and 11 are 0.05 times of the actual ones as the amplitudes of these responses are much larger than those of the other two conditions.

Considering the impacts of the morphing speed, the tip vertical displacements and tip twist are calculated during the morphing process at the flight speed of 50 m/s. The extending and contracting processes at different morphing velocities are studied, respectively. In Figs. 12 and 13, the dimensionless tip vertical displacements and tip twists during the morphing

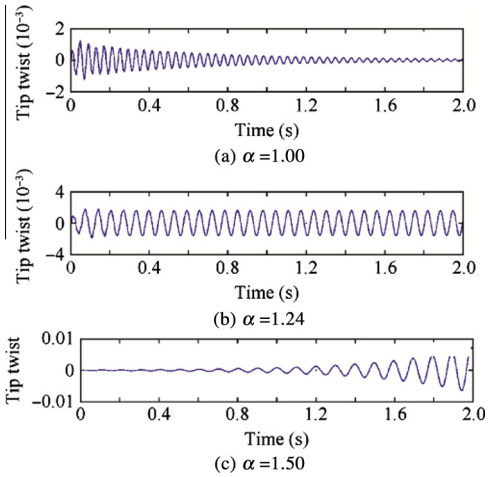

Fig. 11 Tip twist responses with different configurations ($V = 50$ m/s).

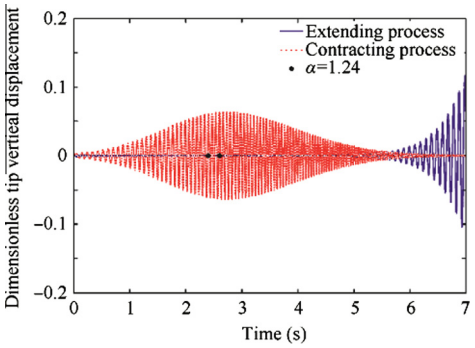

Fig. 12 Tip vertical displacement response during the morphing process ($|\dot{\alpha}| = 0.2$).

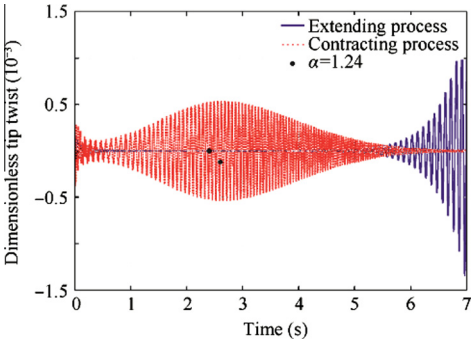

Fig. 13 Tip twist response during the morphing process ($|\dot{\alpha}| = 0.2$).

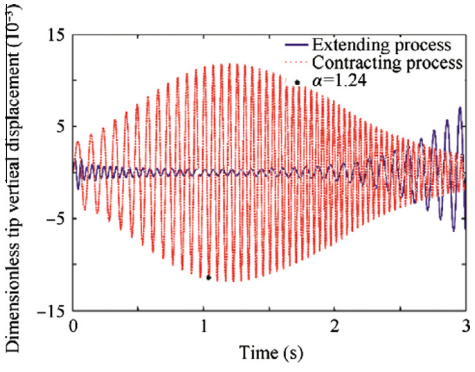

Fig. 14 Tip vertical displacement response during the morphing process ($|\dot{\alpha}| = 0.5$).

process with a morphing speed of $|\dot{\alpha}| = 0.2$ and morphing time of 5 s, as well as the responses after the morphing process, are analyzed for 2 s. During the extending process, the flutter phenomenon occurs after the critical span length $\alpha = 1.24$, i.e., flutter delays. In Section 5.4, one can notice that the positive morphing velocity leads to an increase of the flutter speed, and the amplitudes of responses become so small before the critical span length that, after the flutter point, the divergence process of the oscillations would be slow, which would not be obvious in the figures. During the contracting process, the flutter phenomenon would not disappear after the critical span

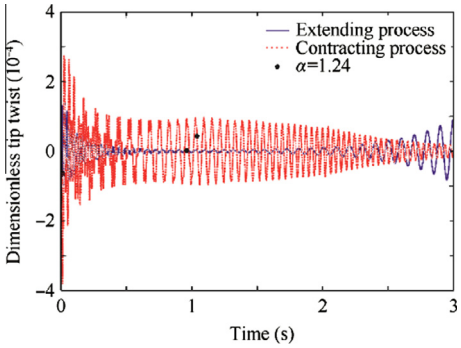

Fig. 15 Tip twist response during the morphing process ($|\dot{\alpha}| = 0.5$).

length $\alpha = 1.24$, and the amplitudes of responses grow fast before the critical points, as the flight speed is much higher than the flutter speed at the initial time when the span length is $1.5l_0$. In this study, we can also notice that changing the wing span length would be an efficient approach for flutter control.

Figs. 14 and 15 show the time histories of oscillations when the morphing speed increases to $|\dot{\alpha}| = 0.5$. The trends of responses are similar to the last case. The amplitudes of the responses are smaller than those at a morphing speed of $|\dot{\alpha}| = 0.2$, which means that faster morphing would improve the aeroelastic response characteristics. However, the energy consumption would be much higher, which leads to more complex actuators and morphing mechanism being needed.

6. Conclusions

(1) A first-order, state-space aeroelastic model for variable-span morphing wings has been developed by combining a variable-length Euler–Bernoulli beam model with a reduced-order unsteady vortex lattice model in this paper. It takes into account the impacts of changeable wing span length and various morphing speeds on the aeroelastic characteristics.

(2) The numerical examples show that the critical flutter speed of the variable-span wing is very sensitive to the span length since it has remarkable effects on structural rigidity properties and aerodynamic characteristics. The flutter speed increases with increasing morphing speed during the extending process, while decreases during the contracting process. That's because the morphing motion can change structural rigidity properties and structural damping which have strong effects on the flutter characteristics.

(3) In addition, the transient aeroelastic responses during the morphing process show that the morphing technology would be a potential flutter control approach to enhance flight quality.

Acknowledgements

This work was co-supported by Defense Industrial Technology Development Program (Nos: A2120110001 and B2120110011), 111 Project (No. B07009), the National Natural Science Foundation of China (Nos: 90816024 and 10876100).

Appendix A.

The coefficients and matrices in Eq. (12) are defined as follows:

$$H_1 = -\Delta\tilde{x}\boldsymbol{F}_1\tilde{\boldsymbol{K}}_{\mathrm{b}}^{-1}\tilde{\boldsymbol{K}}_{\mathrm{w}}\boldsymbol{K}_{\mathrm{c}}\boldsymbol{D}_{\mathrm{c}}\boldsymbol{S}^{\mathrm{T}} + \boldsymbol{F}_2\tilde{\boldsymbol{K}}_{\mathrm{b}}^{-1}\boldsymbol{S}^{\mathrm{T}} \tag{A1}$$

$$H_2 = \Delta\tilde{x}\boldsymbol{F}_1\tilde{\boldsymbol{K}}_{\mathrm{b}}^{-1}\tilde{\boldsymbol{K}}_{\mathrm{w}}\boldsymbol{K}_{\mathrm{c}}\boldsymbol{D}_{\mathrm{c}}\boldsymbol{D}_{\mathrm{a}} - \boldsymbol{F}_2\tilde{\boldsymbol{K}}_{\mathrm{b}}^{-1}\boldsymbol{D}_{\mathrm{a}} + \Delta\tilde{x}\boldsymbol{F}_2\tilde{\boldsymbol{K}}_{\mathrm{b}}^{-1}\tilde{\boldsymbol{K}}_{\mathrm{w}}\boldsymbol{K}_{\mathrm{c}}\boldsymbol{D}_{\mathrm{c}}\boldsymbol{S}^{\mathrm{T}} \tag{A2}$$

$$H_3 = \boldsymbol{F}_1\tilde{\boldsymbol{K}}_{\mathrm{b}}^{-1}\boldsymbol{S}^{\mathrm{T}} \tag{A3}$$

$$H_4 = -\boldsymbol{F}_1\tilde{\boldsymbol{K}}_{\mathrm{b}}^{-1}\boldsymbol{D}_{\mathrm{a}} + \Delta\tilde{x}\boldsymbol{F}_1\tilde{\boldsymbol{K}}_{\mathrm{b}}^{-1}\tilde{\boldsymbol{K}}_{\mathrm{w}}\boldsymbol{K}_{\mathrm{c}}\boldsymbol{D}_{\mathrm{c}}\boldsymbol{S}^{\mathrm{T}} - \boldsymbol{F}_2\tilde{\boldsymbol{K}}_{\mathrm{b}}^{-1}\boldsymbol{S}^{\mathrm{T}} \tag{A4}$$

$$H_5 = -\boldsymbol{F}_1\tilde{\boldsymbol{K}}_{\mathrm{b}}^{-1}\boldsymbol{S}^{\mathrm{T}} \tag{A5}$$

$$\boldsymbol{H}_6 = \boldsymbol{F}_2\tilde{\boldsymbol{K}}_{\mathrm{b}}^{-1}\tilde{\boldsymbol{K}}_{\mathrm{w}}\boldsymbol{\Psi}_R \tag{A6}$$

$$\boldsymbol{H}_7 = \boldsymbol{F}_1\tilde{\boldsymbol{K}}_{\mathrm{b}}^{-1}\tilde{\boldsymbol{K}}_{\mathrm{w}}\boldsymbol{\Psi}_R \tag{A7}$$

$$J_1 = -\Delta\tilde{x}\boldsymbol{G}_1\tilde{\boldsymbol{K}}_{\mathrm{b}}^{-1}\tilde{\boldsymbol{K}}_{\mathrm{w}}\boldsymbol{K}_{\mathrm{c}}\boldsymbol{D}_{\mathrm{c}}\boldsymbol{S}^{\mathrm{T}} + \boldsymbol{G}_2\tilde{\boldsymbol{K}}_{\mathrm{b}}^{-1}\boldsymbol{S}^{\mathrm{T}} \tag{A8}$$

$$J_2 = \Delta\tilde{x}\boldsymbol{G}_1\tilde{\boldsymbol{K}}_{\mathrm{b}}^{-1}\tilde{\boldsymbol{K}}_{\mathrm{w}}\boldsymbol{K}_{\mathrm{c}}\boldsymbol{D}_{\mathrm{c}}\boldsymbol{D}_{\mathrm{a}} - \boldsymbol{G}_2\tilde{\boldsymbol{K}}_{\mathrm{b}}^{-1}\boldsymbol{D}_{\mathrm{a}} + \Delta\tilde{x}\boldsymbol{G}_2\tilde{\boldsymbol{K}}_{\mathrm{b}}^{-1}\tilde{\boldsymbol{K}}_{\mathrm{w}}\boldsymbol{K}_{\mathrm{c}}\boldsymbol{D}_{\mathrm{c}}\boldsymbol{S}^{\mathrm{T}} \tag{A9}$$

$$J_3 = \boldsymbol{G}_1\tilde{\boldsymbol{K}}_{\mathrm{b}}^{-1}\boldsymbol{S}^{\mathrm{T}} \tag{A10}$$

$$J_4 = -\boldsymbol{G}_1\tilde{\boldsymbol{K}}_{\mathrm{b}}^{-1}\boldsymbol{D}_{\mathrm{a}} + \Delta\tilde{x}\boldsymbol{G}_1\tilde{\boldsymbol{K}}_{\mathrm{b}}^{-1}\tilde{\boldsymbol{K}}_{\mathrm{w}}\boldsymbol{K}_{\mathrm{c}}\boldsymbol{D}_{\mathrm{c}}\boldsymbol{S}^{\mathrm{T}} - \boldsymbol{G}_2\tilde{\boldsymbol{K}}_{\mathrm{b}}^{-1}\boldsymbol{S}^{\mathrm{T}} \tag{A11}$$

$$J_5 = -\boldsymbol{G}_1\tilde{\boldsymbol{K}}_{\mathrm{b}}^{-1}\boldsymbol{S}^{\mathrm{T}} \tag{A12}$$

$$\boldsymbol{J}_6 = \boldsymbol{G}_2\tilde{\boldsymbol{K}}_{\mathrm{b}}^{-1}\tilde{\boldsymbol{K}}_{\mathrm{w}}\boldsymbol{\Psi}_{\mathrm{R}} \tag{A13}$$

$$\boldsymbol{J}_7 = \boldsymbol{G}_1\tilde{\boldsymbol{K}}_{\mathrm{b}}^{-1}\tilde{\boldsymbol{K}}_{\mathrm{w}}\boldsymbol{\Psi}_R \tag{A14}$$

The matrices and vectors in Eq. (16) are defined as:

$$\boldsymbol{M}_{\mathrm{s}} = \alpha^4\begin{bmatrix}\boldsymbol{I}_{N_w} & -\bar{x}_\alpha\boldsymbol{A}_1\\ -\bar{x}_\alpha\boldsymbol{A}_1^{\mathrm{T}} & r_\alpha^2\boldsymbol{I}_{N_\theta}.\end{bmatrix} \tag{A15}$$

$$\boldsymbol{M}_{\mathrm{a}} = \frac{\alpha^4}{\pi\mu}\begin{bmatrix}H_1\boldsymbol{I}_{N_w} & H_2\boldsymbol{A}_1\\ J_1\boldsymbol{A}_1^{\mathrm{T}} & J_2\boldsymbol{I}_{N_\theta}.\end{bmatrix} \tag{A16}$$

$$\boldsymbol{C}_{\mathrm{s}} = 2\dot{\alpha}\alpha^3\begin{bmatrix}\boldsymbol{A}_2 & \boldsymbol{A}_3\\ \boldsymbol{A}_4 & \boldsymbol{A}_5.\end{bmatrix} \tag{A17}$$

$$\boldsymbol{C}_{\mathrm{a}} = \frac{\alpha^4}{\pi\mu}\begin{bmatrix}H_3\boldsymbol{I}_{N_w} & H_4\boldsymbol{A}_1\\ J_3\boldsymbol{A}_1^{\mathrm{T}} & J_4\boldsymbol{I}_{N_\theta}.\end{bmatrix} \tag{A18}$$

$$\boldsymbol{K}_{\mathrm{s}} = \begin{bmatrix}\boldsymbol{K}_{\mathrm{s},11} & \boldsymbol{K}_{\mathrm{s},12}\\ \boldsymbol{K}_{\mathrm{s},21} & \boldsymbol{K}_{\mathrm{s},22}.\end{bmatrix} \tag{A19}$$

$$\boldsymbol{K}_{\mathrm{a}} = \frac{\alpha^4}{\pi\mu}\begin{bmatrix}\boldsymbol{0} & H_5\boldsymbol{A}_1\\ \boldsymbol{0} & J_5\boldsymbol{I}_{N_\theta}.\end{bmatrix} \tag{A20}$$

$$\boldsymbol{D} = \frac{\alpha^4}{\pi\mu}\begin{bmatrix}\boldsymbol{A}_{12}\boldsymbol{H}_6\\ \boldsymbol{A}_{13}\boldsymbol{J}_6.\end{bmatrix} \tag{A21}$$

$$\boldsymbol{E} = \frac{\alpha^4}{\pi\mu}\begin{bmatrix}\boldsymbol{A}_{12}\boldsymbol{H}_7\\ \boldsymbol{A}_{13}\boldsymbol{J}_7.\end{bmatrix} \tag{A22}$$

where

$$\boldsymbol{K}_{\mathrm{s},11} = \alpha^2(\ddot{\alpha}\alpha - \dot{\alpha}^2)\boldsymbol{A}_2 + \alpha^2\dot{\alpha}^2\boldsymbol{A}_6 + k_w^2\boldsymbol{A}_7,$$
$$\boldsymbol{K}_{\mathrm{s},12} = -\tilde{x}_\alpha(\alpha^2(\ddot{\alpha}\alpha - \dot{\alpha}^2)\boldsymbol{A}_3 + \alpha^2\dot{\alpha}^2\boldsymbol{A}_8),$$
$$\boldsymbol{K}_{\mathrm{s},21} = -\tilde{x}_\alpha(\alpha^2(\ddot{\alpha}\alpha - \dot{\alpha}^2)\boldsymbol{A}_4 + \alpha^2\dot{\alpha}^2\boldsymbol{A}_9),$$
$$\boldsymbol{K}_{\mathrm{s},22} = \tilde{r}_\alpha^2(\alpha^2(\ddot{\alpha}\alpha - \dot{\alpha}^2)\boldsymbol{A}_5 + \alpha^2\dot{\alpha}^2\boldsymbol{A}_{10}) + k_\theta^2\boldsymbol{A}_{11},$$

and

$$\boldsymbol{A}_1 = \int_0^1 \boldsymbol{v}^{\mathrm{T}}\boldsymbol{\Theta}\mathrm{d}\tilde{y}, \quad \boldsymbol{A}_2 = \int_0^1 (1-\tilde{y})\boldsymbol{v}^{\mathrm{T}}\boldsymbol{v}'\mathrm{d}\tilde{y},$$
$$\boldsymbol{A}_3 = \int_0^1 (1-\tilde{y})\boldsymbol{v}^{\mathrm{T}}\boldsymbol{\Theta}'\mathrm{d}\tilde{y}, \quad \boldsymbol{A}_4 = \int_0^1 (1-\tilde{y})\boldsymbol{\Theta}^{\mathrm{T}}\boldsymbol{v}'\mathrm{d}\tilde{y},$$
$$\boldsymbol{A}_5 = \int_0^1 (1-\tilde{y})\boldsymbol{\Theta}^{\mathrm{T}}\boldsymbol{\Theta}'\mathrm{d}\tilde{y}, \quad \boldsymbol{A}_6 = \int_0^1 (1-\tilde{y})^2\boldsymbol{v}^{\mathrm{T}}\boldsymbol{v}''\mathrm{d}\tilde{y},$$
$$\boldsymbol{A}_7 = \int_0^1 \boldsymbol{v}^{\mathrm{T}}\boldsymbol{v}''''\mathrm{d}\tilde{y}, \quad \boldsymbol{A}_8 = \int_0^1 (1-\tilde{y})^2\boldsymbol{v}^{\mathrm{T}}\boldsymbol{\Theta}''\mathrm{d}\tilde{y},$$
$$\boldsymbol{A}_9 = \int_0^1 (1-\tilde{y})^2\boldsymbol{\Theta}^{\mathrm{T}}\boldsymbol{v}''\mathrm{d}\tilde{y}, \quad \boldsymbol{A}_{10} = \int_0^1 (1-\tilde{y})^2\boldsymbol{\Theta}^{\mathrm{T}}\boldsymbol{\Theta}''\mathrm{d}\tilde{y},$$
$$\boldsymbol{A}_{11} = \int_0^1 \boldsymbol{\Theta}^{\mathrm{T}}\boldsymbol{\Theta}''\mathrm{d}\tilde{y}, \quad \boldsymbol{A}_{12} = \int_0^1 \boldsymbol{v}^{\mathrm{T}}\mathrm{d}\tilde{y}, \quad \boldsymbol{A}_{13} = \int_0^1 \boldsymbol{\Theta}^{\mathrm{T}}\mathrm{d}\tilde{y}.$$

References

1. Wilson JR. Morphing UAVs change the shape of warfare. *Aerosp Am* 2004;**42**(2):28–9.
2. Rodriguez AR. Morphing aircraft technology survey. AIAA-2007-1258; 2007.
3. Barbarino S, Bilgen O, Ajaj RM, Friswell MI, Inman DJ. A review of morphing aircraft. *J Intell Mater Syst Struct* 2011;**22**(9):823–77.
4. Zhang P, Zhou L, Qiu T. A new flexible honeycomb structure and its application in structure design of morphing aircraft. *Acta Aeronaut Astronaut Sin* 2011;**32**(1):156–63 [Chinese].
5. Chen Q, Yin WL, Bai P, Leng JS, Liu ZQ. System design and characteristics analysis of a variable-sweep and variable-span wing-body. *Acta Aeronaut Astronaut Sin* 2010;**31**(3):506–13 [Chinese].
6. Lee DH, Weisshaar TA. Aeroelastic studies on a folding wing configuration; 2005. Report No.: AIAA-2005–1996.
7. Tang DM, Dowell EH. Theoretical and experimental aeroelastic study for folding wing structures. *J Aircraft* 2008;**45**(4):1136–47.
8. Snyder MP, Sanders B, Eastep FE, Frank GJ. Vibration and flutter characteristics of a folding wing. *J Aircraft* 2009;**46**(3):791–9.
9. Liska S, Dowell EH. Continuum aeroelastic model for a folding wing configuration. *AIAA J* 2009;**47**(10):2350–8.
10. Liu DD, Chen PC, Zhang Z, Wang Z, Yang S, Lee DH, et al. Continuous dynamic simulation for morphing wing aeroelasticity; 2009. Report No.: AIAA-2009–2572.
11. Zhao YH, Hu HY. Parameterized aeroelastic modeling and flutter analysis for a folding wing. *J Sound Vib* 2012;**331**(2):308–24.
12. Zhao YH, Hu HY. Prediction of transient responses of a folding wing during the morphing process. *Aerosp Sci Technol* 2011;**24**(1):89–94.
13. Scarlett JN. Multibody dynamic aeroelastic simulation of a folding wing aircraft; 2006. Report No.: AIAA-2006–2135.
14. Yue T, Wang LX, Ai JQ. Longitudinal multibody dynamic characteristics of Z-wing morphing aircraft. *Acta Aeronaut Astronaut Sin* 2010;**31**(4):679–86 [Chinese].
15. Bae JS, Seigler TM, Inman DJ. Aerodynamic and static aeroelastic characteristics of a variable-span morphing wing. *J Aircraft* 2005;**42**(2):528–34.

16. Wang HB, Wang HP. Influence of an axial speed on extendible wing's flutter stability. *Aeronaut Comput Tech* 2012;**42**(2):16–9 [Chinese].
17. Katz J, Plotkin A. Unsteady incompressible potential flow*Low speed aerodynamics: from wing theory to panel method*. New York: McGraw-Hill; 1991. p. 421–511.
18. Zhao YH, Hu HY. Aeroelastic analysis of a non-linear airfoil based on unsteady vortex lattice model. *J Sound Vib* 2004;**276**(3):491–510.
19. Dardel M, Bakhtiari-Neijad F. A reduced order of complete aeroelastic model for limit cycle oscillations. *Aerosp Sci Technol* 2010;**14**(2):95–105.
20. Shams S, Lahidjani MH, Haddadpour H. Nonlinear aeroelastic response of slender wings based on Wagner function. *Thin-Walled Struct* 2008;**46**(11):1192–203.
21. Edwards JW, Wieseman CD. Flutter and divergence analysis using the generalized aeroelastic analysis method. *J Aircraft* 2008;**45**(3):906–15.
22. Shampine LF, Reichelt MW. The MATLAB ODE suite. *SIAM J Sci Comput* 1997;**18**(1):1–22.
23. Goland M. The flutter of a uniform cantilever wing. *J Appl Mech* 1945;**12**(4):A197–208.
24. Hodges DH, Pierce GA. Flutter prediction via assumed modes*Introduction to structural dynamics and aeroelasticity*. Cambridge: Cambridge University Press; 2002. p. 143–6.

Huang Ren is a Ph.D. student in the Institute of Solid Mechanics at Beihang University, where he received his B.S. degree in 2007. His area of research includes structural dynamics and aeroelasticity of morphing aircrafts.

Qiu Zhiping is a professor and Ph.D. advisor in the Institute of Solid Mechanics at Beihang University. He received his Ph.D. degree from Jilin University in 1994. His current research interests are aircraft design, aeroelasticity, structural dynamics, etc.